

Trace constituents of Europa's atmosphere

T.A. Cassidy*, R.E. Johnson, O.J. Tucker

University of Virginia, P.O. Box 3818, Charlottesville, VA 22903-0818, USA

ARTICLE INFO

Article history:

Received 6 August 2008

Revised 15 December 2008

Accepted 16 December 2008

Available online 7 January 2009

Keywords:

Europa

Atmospheres, dynamics

Satellites, atmospheres

Ices

ABSTRACT

Europa is bombarded by intense radiation that erodes the surface, launching molecules into a thin “atmosphere” representative of surface composition. In addition to atoms and molecules created in the mostly water ice surface such as H₂O, O₂, H₂, the atmosphere is known to have species representative of trace surface materials. These trace species are carried off with the 10–10⁴ H₂O molecules ejected by each energetic heavy ion, a process we have simulated using molecular dynamics. Using the results of those simulations, we found that a neutral mass spectrometer orbiting ~100 km above the surface could detect species with surface concentrations above ~0.03%. We have also modeled the atmospheric spatial structure of the volatile species CO₂ and SO₂ under a variety of assumptions. Detections of these species with moderate time and space resolution would allow us to constrain surface composition, chemistry and to study space weathering processes.

© 2009 Elsevier Inc. All rights reserved.

1. Introduction

Jupiter's moon Europa has a tenuous atmosphere. It was first postulated to exist in the 1970s (Steklov, 1977; Yung and McElroy, 1977) and has the observed species O₂ (Hall et al., 1995), H or H₂ (Mauk et al., 2003), Na (Brown and Hill, 1996), K (Brown, 2001), and, via pickup ions, SO₂ and Cl (Volwerk et al., 2001). The erosion of Europa's predominantly water ice surface by robust plasma bombardment (e.g., Cooper et al., 2001) is expected to produce additional atmospheric components (e.g., Johnson et al., 1998, 2004). Energetic heavy ions (sulfur and oxygen) from Jupiter's magnetosphere eject H₂O molecules from the surface in a process called sputtering. Ions, along with electrons and photons, also break molecular bonds. The subsequent chemistry in the ice produces the observed volatiles O₂ and H/H₂ (e.g., Burger and Johnson, 2004; Smyth and Marconi, 2006). O, H and OH are predicted dissociation products of atmospheric H₂O, O₂ and H₂ (Shematovich et al., 2005). Other species expected to be present in the atmosphere are trace species in the surface that get sputtered along with the dominant H₂O. One of these, Na, is by far the best-observed and modeled component of Europa's atmosphere (e.g., Leblanc et al., 2005; Cassidy et al., 2008). Though it is much less abundant than the predicted water-related species, Na is much easier to observe because it fluoresces in sunlight.

This paper describes the issues involved in modeling trace species sputtered from Europa's surface and presents model atmospheres of two volatiles seen in Europa's surface: CO₂ and

SO₂. CO₂ has not been detected in Europa's atmosphere, though it is abundant in Callisto's atmosphere (Liang et al., 2005), and SO₂ has only been detected once via the cyclotron waves produced when it is ionized and picked up by the magnetosphere (Volwerk et al., 2001). These interesting species provide an opportunity to discuss aspects of atmospheric modeling that have not been adequately treated before. The ultimate goal is to learn how atmospheric composition is related to surface composition, chemistry, and space-weathering processes. For example, studies of the Na and K atmospheres suggest that they might originate from Europa's subsurface ocean (Brown, 2001; Leblanc et al., 2002; Johnson et al., 2002) and, if that is the case, then there must be other species present that are indicative of the composition of the ocean.

2. Atmospheric model

We used a Monte Carlo ballistic (collisionless) model of the atmosphere. The Monte Carlo model uses tens of thousands of test particles in order to represent the atmosphere. In this section we describe the atmospheric source processes, loss processes and interactions with the surface. In order to calculate densities (and column densities) I assume that the atmospheric densities are *approximately* constant state over some short period of time.

A formula for the column density N is found by considering the balance between particles entering and exiting a given column:

$$dN/dt = \dot{Q} \bar{f} / \Delta A - N / \Delta t_{av}$$

where \dot{Q} is the global source rate of particles, \bar{f} is the fraction of those particles that enter the column, Δt_{av} is the average time a particle spends in the column, and ΔA is the column area. If

* Corresponding author.

E-mail address: tac2z@virginia.edu (T.A. Cassidy).

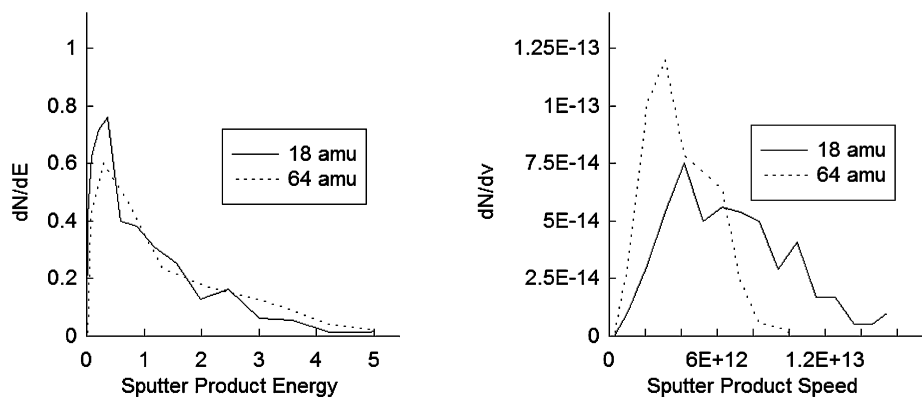


Fig. 1. Normalized speed and energy distributions from a molecular dynamics simulation of electronic sputtering. The matrix material (mass 18) contains a contaminant of mass 64. The sputter product energy on the left-hand side is unitless; it is scaled by the material binding energy. For water ice, a sputter product energy of 1 corresponds to ~ 0.45 eV. The sputter product speed was scaled by the square root of the binding energy; the horizontal axis of the right-hand graph has units of $\text{kg}^{-1/2}$.

the density is unchanging (or nearly so), we can set $dN/dt = 0$ and find N . Because the column density varies as Europa orbits, we estimate column density in a dynamic atmosphere by only calculating densities during a time short enough that N changes little. The simulation times we used ranged from 2 to 50 European days, but densities were only calculated for a few hours around the time period of interest, during which the surface temperatures are approximately constant, surface temperature being the only parameter that changes during the simulation.

In our model the ejection rate of particular species is proportional to its surface concentration. Although the ejection efficiencies for trace species in an ice matrix have not been measured, a molecular dynamics simulation described below suggests that trace species are carried off with the large number, up to 10^4 , of water molecules sputtered by each energetic heavy ion (see also: Johnson et al., 1998).

We also assume that the sputtering rate is spatially uniform, as most of the sputtering on Europa is done by energetic heavy ions (sulfur and oxygen) which impact the surface nearly uniformly (Cooper et al., 2001; Paranicas et al., 2002). This is contrary to what was assumed in earlier models (e.g., Sieveka and Johnson, 1982; Tiscareno and Geissler, 2003). The assumption of a uniform sputtering rate may be undermined by a non-uniform sputtering yield: Europa's surface is not pure water ice. The sputtering yield is, however, likely quite large even at Europa's trailing hemisphere apex, where, although the surface is 90% hydrated non-ice material, H_2O molecules still outnumber other molecules 10 to 1 (Carlson et al., 2005).

The energy distribution of trace species sputtered from water ice has not been measured. Leblanc et al. (2005) used telescopic observations to constrain the energy distribution of Na ejected from Europa (see also: Johnson, 2000). The results are consistent with sputtered Na having either the same energy distribution as laboratory-sputtered H_2O or the same velocity distribution (Cassidy et al., 2008). These observations cannot distinguish between the two cases because Na and H_2O have similar masses. Although the ejection of trace species in a matrix material is now a reasonably well studied process, there is a dearth of results for the energy spectra. Therefore, we carried out molecular dynamics simulations (see, e.g., Bringa et al., 1999) to compare their energy and velocity distributions.

Molecular dynamics (MD) is the simulation of a solid or liquid at the molecular level by numerical integration of the classical equations of motion. The first step in MD modeling is the choice of an appropriate intermolecular potential. We used the Lennard-Jones potential (also known as the 6-12 potential), as it is appropriate for many condensed-gas solids (Bringa et al., 1999). For this simple potential both the yields (number of molecules ejected

per ion incident) and the energy spectra scale with the molecule's binding energy (Fig. 1). Although the Lennard-Jones potential does not accurately describe H_2O 's hydrogen bonding, simulations of large sputtering yields using a variety of intermolecular potentials showed the same scaling: Bringa et al. (1999) found that the use of Lennard-Jones and Morse potentials resulted in nearly identical sputtering yields, as did Tucker et al. (2005) when using an embedded atom potential. Jakas et al. (2002) even found the same using a fluid-dynamic model.

For the matrix material in our MD model we used atoms with mass 18 (the same as H_2O). The trace species was assumed to have identical chemical properties (i.e., the same Lennard-Jones parameters) but with a mass of 64 (the same as SO_2). The passage of an energetic heavy ion through the ice was simulated by imparting kinetic energy to atoms along an ion's path through the solid. The resulting sputter product energy and speed distributions are shown in Fig. 1. These results are scaled to the binding energy, one of the two parameters of the Lennard-Jones potential (Bringa et al., 1999). Therefore, a "sputter product energy" of 1 in Fig. 1 corresponds, for water ice, to its binding energy of ~ 0.45 eV. In Fig. 1 (right) the sputter product speed was scaled by the square root of the binding energy.

Because the energy distribution for the trace species appears to be very similar the matrix material in these model simulations, we will assume that the energy spectrum measured by Reimann et al. (1984) for the sputtering of water ice by heavy ions applies also to the imbedded contaminant. As mentioned above, we also found that trace constituent atoms were roughly sputtered in proportion to their concentration in the solid. These approximations break down for small sputtering yields but are appropriate for the large yields expected at Europa.

Based on the results of Cassidy and Johnson (2005), the exit-angle distribution is assumed to be given by

$$\frac{dP}{d\cos(\theta)} = 2\cos(\theta),$$

where θ is the angle of ejection from Europa's local surface normal.

For these contaminant species ejected from the surface, we include loss by gravitational escape and loss by electron impact ionization and dissociation. Solar UV photons also cause ionization and dissociation, but at much lower rates (Shematovich et al., 2005; Smyth and Marconi, 2006; Johnson et al., 2009). Electron impact ionization and dissociation lifetimes are uncertain and variable due principally to uncertainty in and variability of the electron temperature and density near Europa's surface. To a first approximation, the magnetospheric electron population of ~ 20 eV

Table 1
Lifetimes.

	SO ₂ ^a	CO ₂ ^b	H ₂ O ^c	O ₂ ^d	Na ^e
Lifetime against ionization/dissociation (20 eV, 100 cm ⁻³)	1.1 × 10 ⁵ s	2.2 × 10 ⁵ s	1.5 × 10 ⁵ s	2.3 × 10 ⁵ s	9.8 × 10 ⁴ s
Lifetime against ionization/dissociation (10 eV, 100 cm ⁻³)	3.6 × 10 ⁵ s	8.4 × 10 ⁵ s	4.2 × 10 ⁵ s	6.6 × 10 ⁵ s	1.3 × 10 ⁵ s
Lifetime against ionization/dissociation (1 eV, 10 ⁴ cm ⁻³)	4.0 × 10 ⁵ s	7.7 × 10 ⁵ s	1.0 × 10 ⁹ s	2.0 × 10 ⁹ s	2.9 × 10 ⁵ s

Lifetimes calculate from electron densities, speeds and cross sections.

^a Cross sections from Lindsay et al. (1996).

^b Cross sections from Hudson et al. (2004).

^c Cross sections from Itikawa and Mason (2005).

^d Cross sections from Cosby (1993) and Straub et al. (1996).

^e Cross sections from Johnston and Burrow (1995).

electrons is assumed to be unchanged as they pass near the surface (Hall et al., 1998). Lifetimes used in the model for SO₂ and CO₂ are shown in Table 1. For our model atmospheres, lifetimes were calculated using lab-measured cross sections, an assumed electron temperature of 20 eV, and an assumed electron density of 100 cm⁻³ (Johnson et al., 2009). Given the variability in electron temperature and density, we also show the lifetimes for 10 eV electrons. The difference in lifetimes is significant, but the two sets of lifetimes are of the same order of magnitude. A dense (~10⁴ cm⁻³) ionosphere of “cold” electrons (Kliore et al., 1997; Saur et al., 1998) makes a minor contribution to ionization and dissociation.

Gravitational escape is incorporated by removing particles when they reach Europa's Hill sphere at 8.7 Europa radii, which requires 0.019 eV/amu for a particle launched from the surface. The Hill sphere defines, roughly, the region in which Europa's gravity dominates Jupiter's gravity. Its use approximates the effects of Jupiter's gravity, which is otherwise neglected. While Jupiter's gravity is important in modeling the extended atmosphere and neutral torus (e.g., Leblanc et al., 2005), it is not significant in the near-surface region that we consider in this paper (Tiscareno and Geissler, 2003). The fraction of molecules ejected from the surface that reach the Hill sphere depends on the ejection process. With the exception of H₂, a negligible fraction of *thermally desorbed* molecules will reach escape energy. The fraction of *sputtered molecules* with escape energy is significant given H₂O's energy spectrum (Reimann et al., 1984; Shematovich et al., 2005). This is very roughly given by:

$$\frac{dP}{dE} \approx \frac{2UE}{(E+U)^3} \quad (1)$$

where dP is the probability of a particle leaving the surface with an energy between E and $E + dE$ and U , a laboratory measured parameter, is ~0.055 eV.

Assuming that SO₂ and CO₂ sputtered along with the H₂O matrix material have roughly the same energy distribution as sputtered H₂O when the sputtering yields are large, then about 9% (SO₂) and 12% (CO₂) reach the Hill sphere. In these simulations we track sputtered molecules in the gas phase, their redistribution across Europa's surface and their residence time in the regolith before being either thermally desorbed or again sputtered. Therefore, the overall importance of gravitational escape is affected by the multiple sputter ejections in a typical molecule's lifetime.

The average sputtering rate of H₂O at Europa has been estimated many times, most recently by Paranicas et al. (2002). He estimated a globally-uniform sputtering rate of 7×10^9 cm⁻² s⁻¹, a value we use here. This rate can be converted to the lifetime of a surface molecule against sputtering of 1.3×10^5 s and is roughly independent of latitude and longitude. The thermally produced portion of the H₂O atmosphere is negligible: it has, at its subsolar peak, a column density two orders of magnitude smaller than the sputtered H₂O atmosphere (see also: Cooper et al., 2001).

Tiscareno and Geissler (2003) considered the possibility of non-uniform H₂O sputtering in an effort to explain Europa's leading-trailing color asymmetry. They hypothesized that the asymmetry was due to a net burial of species on the leading hemisphere by H₂O sputtered from the trailing hemisphere. However, their case B, which had the most realistic parameters, resulted in no net H₂O redistribution, consistent with the assumptions made here for sputter ejection.

A numerical issue regarding the atmospheric source rate arises due to the nature of our program: we follow particles throughout their lifetimes from the initial sputtering through loss, including, for refractory species such as H₂O, several returns to the surface and subsequent *re-sputtering*. The problem with re-sputtering means that our program effectively multiplies the sputtering yield; for instance, H₂O molecules in our program are sputtered, on average, 3 times before being lost. If we assume that H₂O molecules are initially sputtered at the rate listed above, then the model, by re-sputtering the H₂O an additional two times, effectively triples the sputtering rate. We account for this by lowering the sputtering rates by a factor of 3. We do the same for trace species, even though they will not generally get sputtered 3 times. The reason for this can be found by looking at the problem another way: the sputtering rate needs to be reduced because returning water molecules cover the surface and thus partially protect it from sputtering. We divide by 3 because H₂O is the primary sputter product and thus is primarily responsible for covering the surface.

As mentioned above we include two competing ejection processes; sputtering and thermal desorption. Fig. 2 shows the residence time on the surface, the average time before thermal desorption, for a variety of species. The figure's temperature range extends from polar to subsolar temperatures. O₂, with its short residence time at all Europa temperatures, will almost always thermally desorb before being sputtered while H₂O will only rarely thermally desorb before being sputtered. This is usually implemented in atmospheric models by using a “sticking coefficient” of 0 for O₂ and 1 for H₂O. For SO₂ and CO₂, the relative importance of sputtering and thermal desorption will vary during a European day. These lifetimes are turned into probabilities in our Monte Carlo model. A molecule that has returned to the surface from the atmosphere has a probability $1 - \exp[-\Delta t/\tau_S]$ of desorbing and probability $1 - \exp[-\Delta t/\tau_D]$ of sputtering (or, rather, *re-sputtering*) during a time Δt . Here τ_S and τ_D are the residence times against sputtering and thermal desorption, respectively.

The residence times for a molecule on a grain surface in Fig. 2 come from Sandford and Allamandola (1993), except for the O₂ curve, which came from Shi et al. (2007). There was no data available for SO₂ on H₂O ice, so we used the SO₂ on SO₂ curve. The use of the SO₂ on SO₂ residence time curve is partly justified by the similarity of the CO₂ on CO₂ curve and the CO₂ on H₂O curve (not shown; Sandford and Allamandola, 1993). However, it is possible that the SO₂ on SO₂ curve is quite different from the SO₂ on H₂O curve. Further experimental data is needed to resolve this ques-

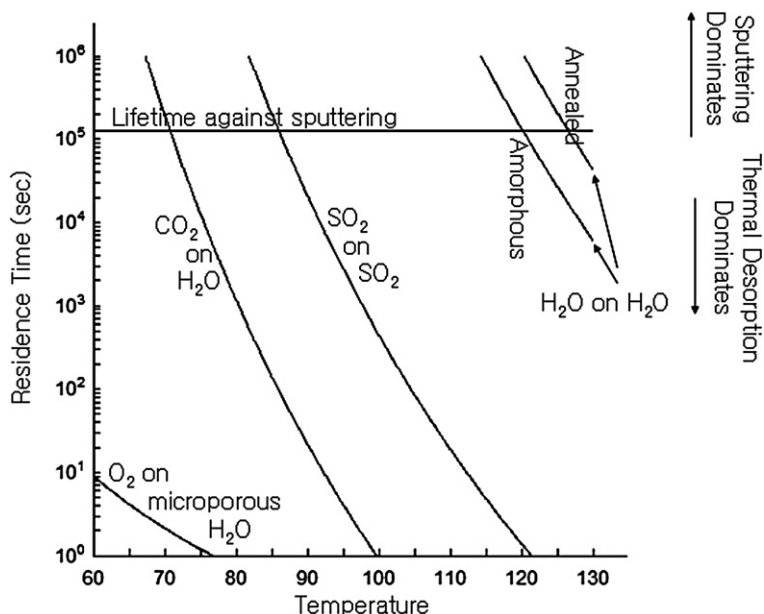


Fig. 2. Residence time as a function of temperature for a variety of species. For residence times above the horizontal line labeled “lifetime against sputtering,” a molecule is more likely to be sputtered or photodesorbed along with H₂O before being thermally desorbed. All data come from Sandford and Allamandola (1993), except for the O₂, which comes from Shi et al. (2007), and the “lifetime against sputtering,” which comes from Paranicas et al. (2002).

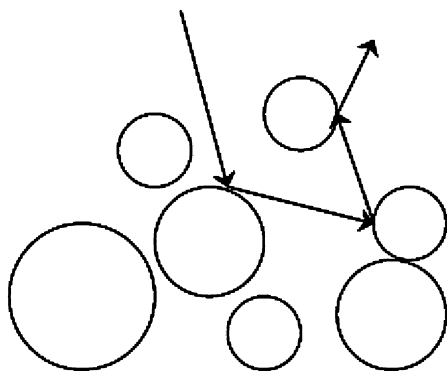


Fig. 3. Schematic of an atmospheric molecule entering and leaving the regolith.

tion, and, as discussed later, a laboratory measurement on pure H₂O might not be applicable at Europa's surface. The O₂ curve (Shi et al., 2007) may be considered an upper limit to O₂'s residence time since the data was acquired using “microporous” water ice; ice that is porous at the scale of nanometers (as distinguished from regolith porosity). Using this data with our model requires that atmospheric molecules are fully thermally accommodated in the brief period when they are adsorbed on the surface.

This begs the question: why would the SO₂ and CO₂ known to be present in the surface need to be sputtered when they should, according to Fig. 2, be desorbed? This is an unanswered question addressed by Hand et al. (2006) and Hibbitts et al. (2004). We consider two possibilities: first, that these volatile molecules, once liberated by sputtering, are well described by Fig. 2, and, second, that the residence times are much longer than the laboratory measurements shown in Fig. 2.

Europa's porous regolith (Simonelli and Buratti, 2004) complicates these ejection processes. A molecule sputtered or desorbed from within the regolith might hit the underside of a regolith grain, rather than exit the surface, where it would be protected from sputtering (Cassidy and Johnson, 2005). It also increases the residence time since a molecule may be repeatedly adsorbed and desorbed deep within the regolith (Hodges, 1980). This is shown schematically in Fig. 3.

The average time a molecule spends in a regolith, as a function of regolith depth, was calculated two ways. A molecule entering the regolith from the atmosphere can be approximated by a 1-D random walk of m steps with a reflecting boundary condition to represent the bottom of the regolith (Hodges, 1980). The result is that a molecule is adsorbed and desorbed $2m$ times, on average, before leaving the regolith and so would spend an average time of $2m\tau_D$ in the regolith, where τ is the residence time on a grain surface. A calculation using the Monte Carlo regolith model described by Cassidy and Johnson (2005) found an average time of $\sim 3m\tau_D$, with m being, in this case, a unitless measure of the regolith depth: $m = z/\lambda$, where z is the depth of the regolith and λ is the mean free path, the average distance a molecule travels before hitting a regolith grain. Europa's regolith depth is uncertain, but Cooper et al. (2001) estimated that it was on the order of 1 m deep. If the mean free path is about 1 mm (based on 90% porosity and a regolith grain radius of 100 μm), then 1 m corresponds $m \approx 1000$. That allows us to estimate the average time spent in the regolith, but the median time can be quite different. In our Monte Carlo regolith model the median number of desorptions a particle endures before leaving the regolith never goes above 4, even as the average goes to infinity (Hodges, 1980; Cassidy and Johnson, 2005).

Europa's surface temperatures were obtained from the Spencer et al. (1999) temperature map, which is based on Galileo mission data. The dayside temperature map was fit with the function $40 + 50\cos(i)^{1/4} + 40\cos(i)$ K, where i is the latitude and i is the solar zenith angle. The nightside temperature was fit by the function $40 + 50\cos(i)^{1/4}$ K. The errors on the fit were ± 10 K, although actual errors may be larger due to the reasons discussed by Spencer et al. (1999). An accurate temperature distribution is important because, all other parameters being equal, the column density of a volatile species is anticorrelated with temperature (Hodges, 1980). This effect is not seen in 1-D ballistic atmosphere models, where increasing the surface temperature increases a desorbed particle's speed, and thus particle's ballistic flight time, which increases the column density (Johnson, 1990). The same is true in our 3-D model, but that effect is overwhelmed by another: a molecule desorbed from a high-temperature region travels farther in its ballistic arc than from a low-temperature region so that,

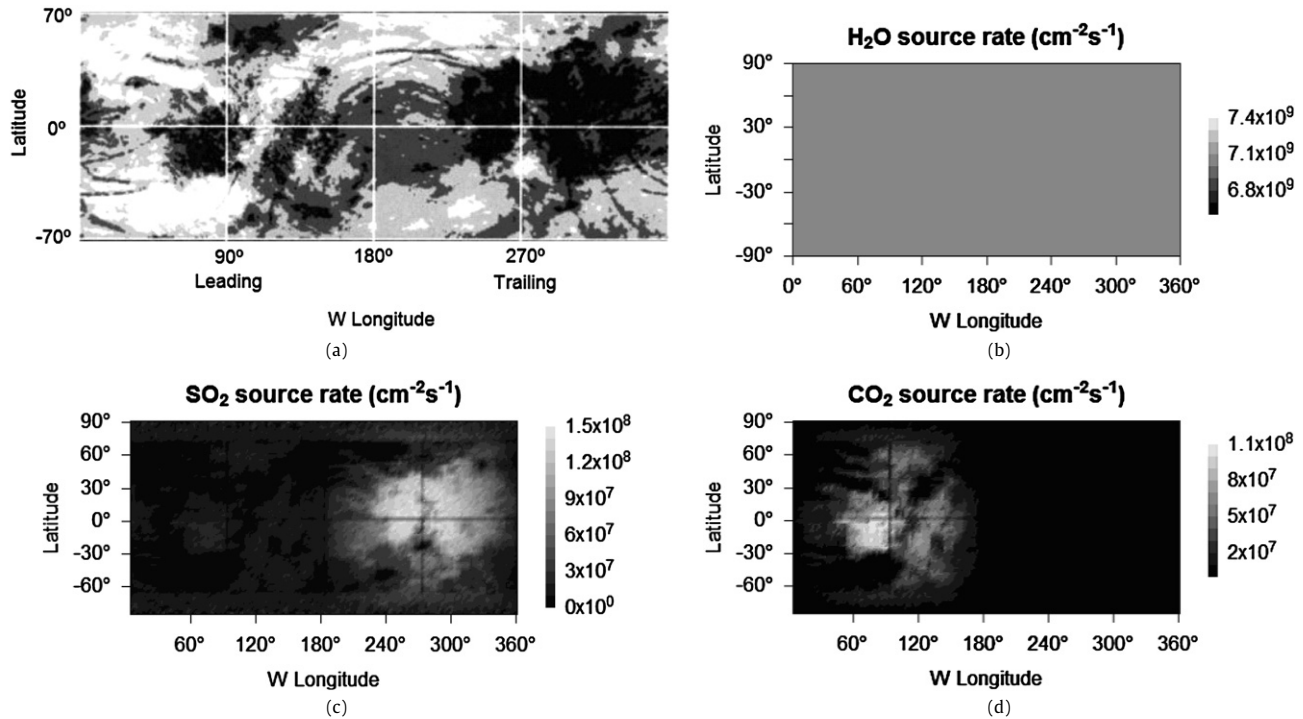


Fig. 4. (a) Map of bright and dark terrain from [McEwen \(1986\)](#). (b) Source rate map for the sputtering of H₂O. As discussed in Section 2, the H₂O sputtering rate is roughly uniform. (c) Source rate map of SO₂ for Figs. 5 and 6. (d) Same as (c) for CO₂. For reasons discussed in the text, the ejection rates used in the model are a factor of 3 lower than the rates shown in this figure.

after many desorptions, the average molecule spends more time in the low temperature region. This result does not apply to species with long residence times like H₂O.

3. Results: Spatial distributions

SO₂ and CO₂ source rates were found by using our conclusion, discussed above, that their sputtering rates are roughly proportional to their concentration along with estimates of their spatially non-uniform surface concentrations. The IUE space telescope first observed the UV absorption attributed to SO₂ ([Lane et al., 1981](#); [Ockert et al., 1987](#)). The absorption's longitudinal trend roughly follows the sulfur implantation pattern calculated by [Pospiezsalska and Johnson \(1989\)](#), with a peak concentration near the apex of the trailing hemisphere (the hemisphere opposite the direction of Europa's orbital motion and upstream of the co-rotating plasma). Europa's sulfate-rich hydrated material and dark terrain have similar distributions and are a possible source of SO₂ via radiolysis ([Carlson et al., 1999, 2005](#)). According to [Carlson \(2004\)](#) and [Carlson et al. \(2009\)](#), the SO₂ is associated with Europa's dark terrain ([Fig. 4](#)), though [Hansen and McCord \(2008\)](#), examining a portion of the trailing hemisphere, found only a weak correlation. We used a map of dark terrain as a proxy for SO₂ concentration.

[McEwen \(1986\)](#) identified 4 shades of dark terrain; from lightest to darkest, we distributed the SO₂ density as 0%, 33%, 67% and 100% of the maximum SO₂ concentration. [McEwen \(1986\)](#) removed an "exogenous" pattern in the dark terrain map but we added it back in as it is similar to the longitudinal trend seen by the IUE and is thought to be the result of sulfur implantation ([Pospiezsalska and Johnson, 1989](#)). [Hand et al. \(2006\)](#) estimated a range of values for the global average SO₂ surface density but chose a nominal value of 0.3% (by number), which we adopted. A map of the SO₂ source rate is shown in [Fig. 4](#).

CO₂ trapped in ice was detected by the Galileo NIMS instrument and its surface density has also been estimated ([Hand et](#)

[al., 2006](#)). Unlike SO₂ it is found preferentially on the leading hemisphere in the dark terrain, consistent with radiolytic production from meteoritic material ([Carlson, 2001, 2004](#); [Carlson et al., 2009](#)). Alternatively, given the dark terrain's association with geological features, it may also be endogenic. There is also some evidence that it is present on the anti-jovian trailing hemisphere ([Hansen and McCord, 2008](#)). For our model's CO₂ distribution we used [McEwen's \(1986\)](#) dark terrain distribution in [Fig. 4a](#) multiplied by the cosine of the angle away from the leading hemisphere apex. We used the [Hand et al.](#) estimate of 0.08% for the globally-averaged surface density. A map of the CO₂ source rate is shown in [Fig. 4](#).

[Fig. 5](#) shows the results of the SO₂ simulation for two times of day, as indicated by the accompanying temperature maps. The SO₂ results show a strong dependence on time of day, with SO₂ column density highest on the daytime hemisphere. This strong dependence on temperature is due to the strong temperature dependence of its residence time ([Fig. 2](#)). A molecule on the night-side, where the temperature is less than 90°, has a residence time comparable to a European day (3×10^5 s) and the lifetime against sputtering (1×10^5 s). An SO₂ molecule in the cold nighttime regions will sit on the surface until daylight or until it is sputtered. Since sputtering is energetic ([Eq. \(1\)](#)), some sputtered molecules will be deposited on the dayside. Also, each time an SO₂ molecule is sputtered it has a ~9% chance of gaining escape energy.

The simulations of CO₂ show a very different behavior: almost no dependence on time of day. The reason for this difference is its volatility; CO₂, unlike SO₂, can be thermally desorbed during the nighttime.

That these volatile species remain in the surface at all is surprising ([Hibbitts et al., 2004](#)). It might be the case that CO₂ and SO₂ have much longer residence times on non-ice materials than shown in [Fig. 2](#). Accordingly we considered the possibility that these molecules adsorb in radiation-produced defects or chemically active sites in Europa's dark terrain. To explore this possibility we ran cases in which SO₂ and CO₂ had infinite residence time on

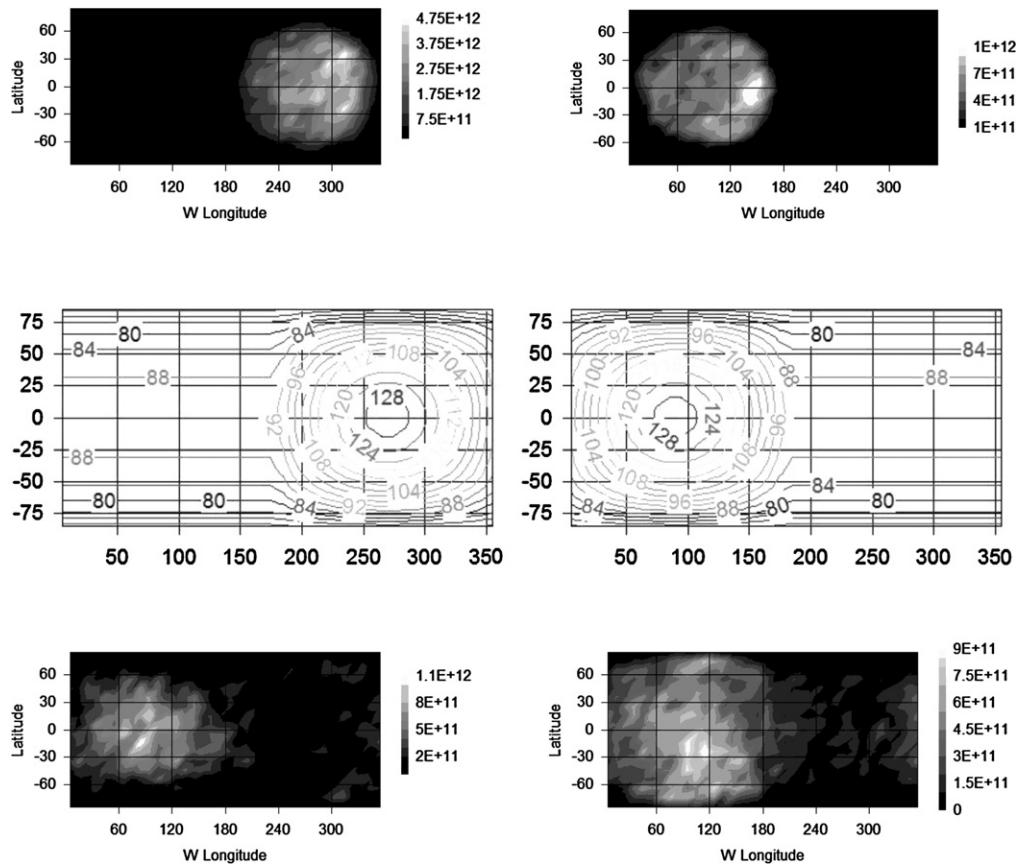


Fig. 5. Top: Atmospheric SO₂ column density for two different times of day (shown by the temperature maps in the middle panel). The SO₂ atmosphere freezes out onto the night side. Bottom: Atmospheric CO₂ column density for the same times of day as the SO₂ above.

McEwen's (1986) two darkest terrains. The result (Fig. 6) is that SO₂ and CO₂ migrate to the bright terrain, as can be seen by comparing Fig. 6 and Fig. 4a.

4. Results: Densities

In this section we calculate the atmospheric density as a function of altitude, paying special attention to the detectability of trace atmospheric species by a spacecraft in orbit above Europa's surface. A low-power, lightweight mass spectrometer might be able to detect neutral densities as low as 100 cm^{-3} (P. Würz, personal communication, 2008), sensitive enough to detect even trace atmospheric constituents.

Density vs. altitude profiles from the SO₂ and CO₂ simulations of Fig. 5 are shown in Fig. 7 along with our estimated H₂O densities and Na densities computed using the "nominal" Na source rate from Leblanc et al. (2005). This graph demonstrates the different types of atmospheres created by sputtering vs. thermal desorption. The atmospheres produced primarily by thermal desorption (SO₂ and CO₂) have very large densities near the surface but fall off quickly with altitude. The atmospheres produced primarily by sputtering (H₂O and Na) have much lower densities at the surface, but the densities decay slowly over the altitude range shown. Slow decay is also seen for SO₂ and CO₂ at higher altitudes where the escaping component becomes a larger fraction of the density. It is seen that a neutral mass spectrometer at $\sim 100 \text{ km}$ altitude can detect all three species, though CO₂ and SO₂ are near our estimated limit of detectability. To detect even less abundant species, that limit might be lowered by integration of data over many orbits. Another way to improve sensitivity is to use the mass spectrometer to measure ion, rather than neutral densities. Since the dominant

atmospheric loss process is ionization, ions representative of atmospheric composition should be abundant (Johnson et al., 1998; Sittler et al., 2008), though modeling their abundance is outside the scope of the present work.

The densities are quite sensitive to the various assumptions discussed above. Accordingly, we calculated SO₂ and CO₂ densities at 100 km altitude using different assumptions to get a range of possible values. The altitude of 100 km was chosen because this is a likely altitude for a spacecraft in orbit (Pappalardo et al., 2007). The results are shown in Table 2, along with density ranges for other species (Leblanc et al., 2005; Shematovich et al., 2005; Smyth and Marconi, 2006). For CO₂ and SO₂, we include the two limiting cases described in the previous section (Figs. 5 and 6) and one additional case in which molecules that return to the surface are lost (eliminated from the simulation). This might be this case if gardening buries molecules deep within the regolith (Cooper et al., 2001), if the molecules are lost through chemical reactions (Cassidy et al., 2007). Such an efficient loss process at the surface is unlikely, but included for the sake of completeness.

The ultimate goal of measuring atmospheric densities is to learn more about the surface. The problem of deducing surface composition from atmospheric densities is simplest for the case of refractory species, such as Na or a complex organic. We calculated density as a function of altitude for several masses using the assumption of long residence times, re-sputtering and an ionization/dissociation rate proportional to the molecular cross section ($\sim \text{mass}^{2/3}$). As seen in Fig. 8, the densities are all similar at 100 km, $\sim 3 \times 10^5 d \text{ cm}^{-3}$, where d is the number fraction of that molecule in the surface. Therefore, a neutral detection threshold on the order of 100 cm^{-3} requires a number fraction of $> \sim 3 \times 10^{-4}$ in the surface.

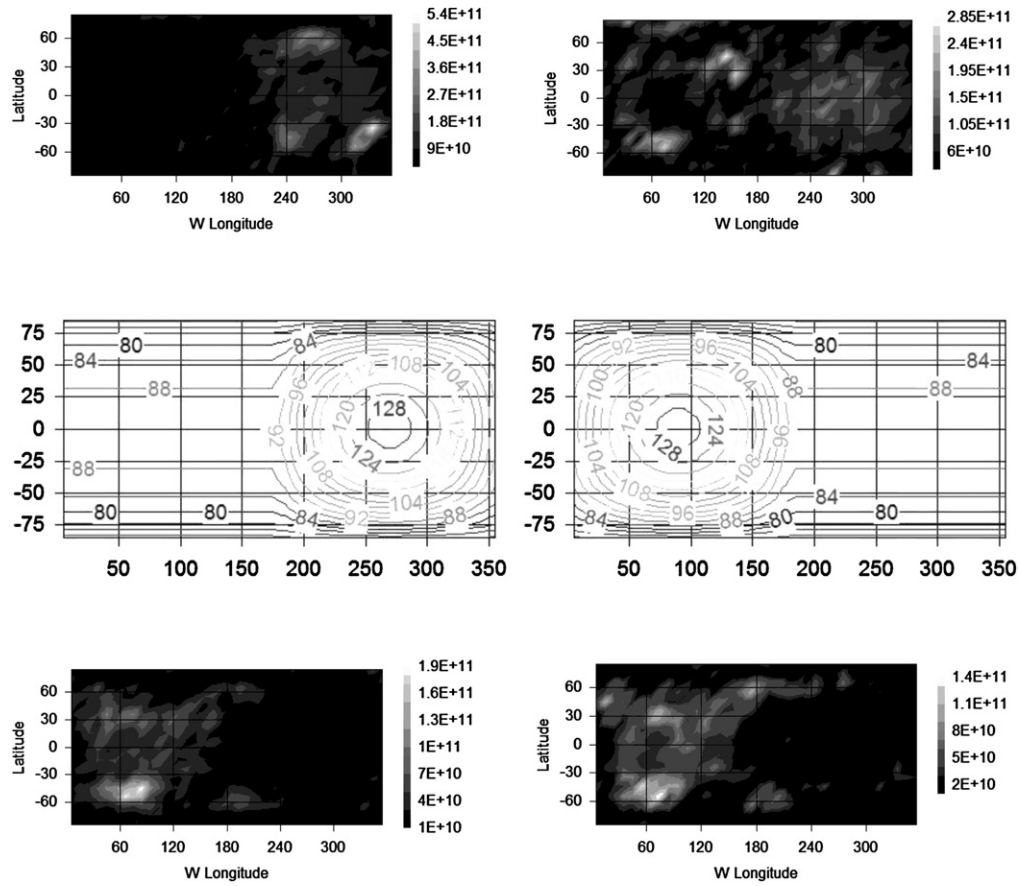


Fig. 6. Same as Fig. 5, but calculated with different residence times. CO₂ and SO₂ freeze (have infinite residence time) on the dark material shown in Fig. 4a. The highest column densities are above the bright terrain.

5. Conclusions

The aim of the modeling described is to connect atmospheric properties to surface properties. An obvious connection is the surface/atmosphere composition, as discussed above. Here we show that it is very likely that the morphology of the atmospheric SO₂ and CO₂ can be mapped by a neutral mass spectrometer on a spacecraft orbiting at ~ 100 km above the surface of Europa. In addition, a comparison of Figs. 5 and 6 shows that the atmospheric morphology can reveal other properties. A long residence time, as indicated by the morphologies seen in Fig. 6, would indicate a strong attraction between molecules and the surface, but, more importantly, it could also indicate a sink for returning atmospheric molecules. That is, the gardening rate, though stochastic, is, on average, faster than the sputtering rate (Cooper et al., 2001). Therefore returning molecules that are adsorbed could be mixed downward and buried deep into the surface over time, eventually reaching the ocean. Such a sink has been hypothesized for the O₂ atmosphere (Johnson et al., 2003) and has astrobiological implications (Hand et al., 2006).

We used a variety of assumptions to explore the connections between Europa's atmosphere and surface. One possible test of these assumptions is found in the extensive work done on simulating Europa's Na atmosphere (Leblanc et al., 2005; Cassidy et al., 2008; Cipriani et al., 2008). Spectral similarity between Na sulfate salts and the hydrated material in Europa's dark terrain allow us to crudely estimate the density of Na in the surface. Based on the discussion above, this should allow us to estimate its abundance in the atmosphere. Orlando et al. (2005) used laboratory spectra of flash-frozen salts to estimate that the hydrate on Europa's sur-

face is $\sim 40\%$ Na₂SO₄·*n*H₂O, but did not estimate density. Carlson et al. (1999) did, however, estimate the density of the hydrate under the assumption that it was hydrated sulfuric acid (H₂SO₄·8H₂O). Combining the two estimates yields a globally-averaged concentration of $\sim 0.5\%$. This, perhaps coincidentally, is the density estimated by Johnson (2000). Using the observationally-constrained estimates of the Na source rate (Leblanc et al., 2005) we estimate a Na surface concentration of 0.08–2.0%. This range was calculated using the Paranicas et al. (2002) H₂O sputtering rate of 7×10^9 cm⁻² s⁻¹, the Leblanc et al. (2005) Na source rate range of 0.5 – 14.4×10^7 cm⁻² s⁻¹ and, of course, the assumption that the sputtering rate of a trace species is proportional to its surface concentration.

This similarity between estimates based on the atmosphere and spectroscopy is compelling but also requires caution: a modeler can employ a wide variety of parameters and assumptions. We considered a variety of possibilities in this paper, resulting in the large range of values shown in Table 2, but did not address some important variables, such as a variation in ion flux due to Europa passing in and out of the jovian magnetosphere's plasma sheet, where electron density and "cold" ion densities are highest. In addition, Paranicas et al. (2002) and Cipriani et al. (2008) found evidence that energetic ion fluxes vary by up to an order of magnitude.

Given the lack of laboratory data, our MD model result that the sputtering rate of a trace species in a condensed-gas matrix is proportional to its concentration needs to be verified for a water ice matrix (Carlson et al., 2009). Further laboratory work and MD simulations will constrain these numbers, but it will take a neutral mass spectrometer near Europa to settle questions about surface

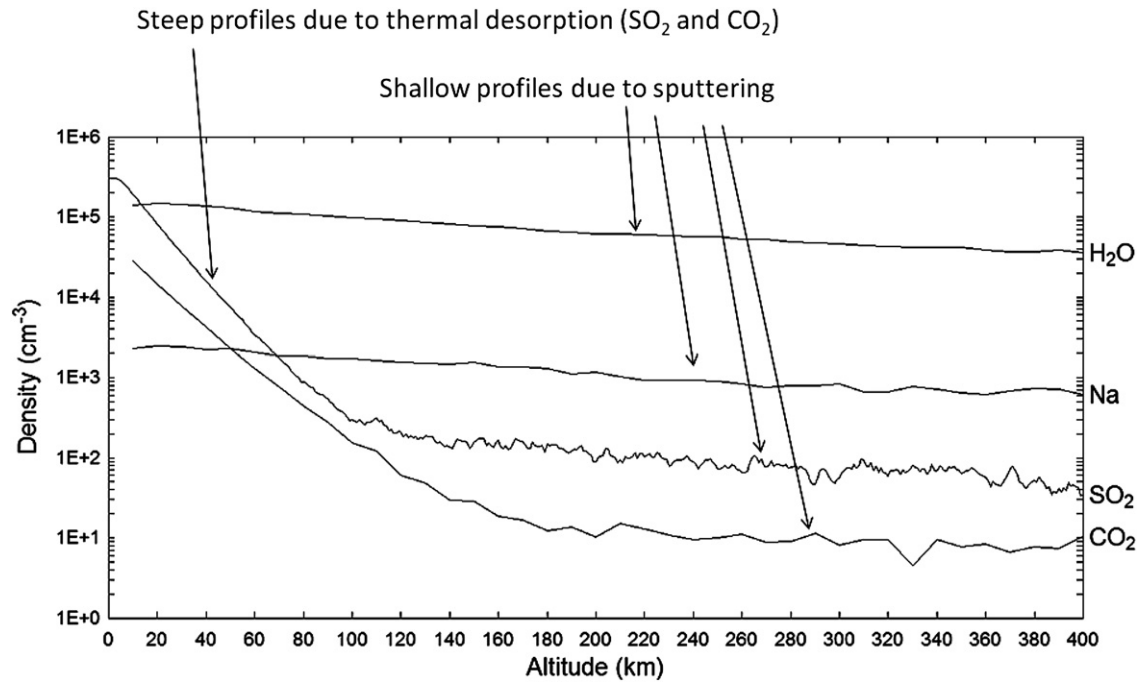


Fig. 7. Neutral density vs. altitude for selected species and cases. The detection threshold is an estimate from P. Wurz (personal communication). The shallow profiles still decay much faster than $1/r^2$.

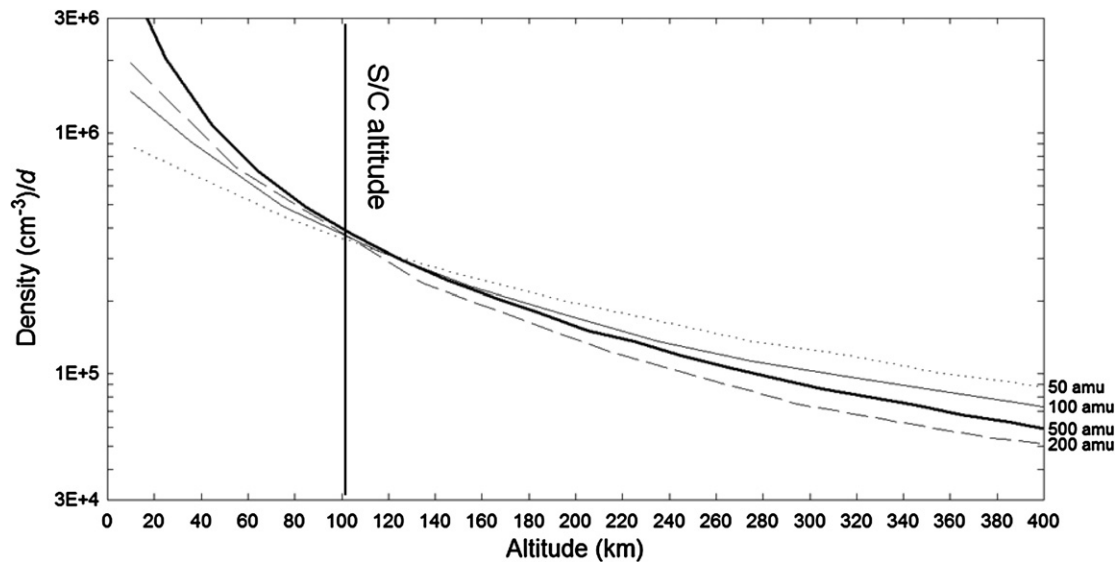


Fig. 8. Density vs. altitude for refractory molecules of different masses. The density of a given atmospheric species with a number fraction d in the surface is given by multiplying the plotted density times d . This allows us to estimate the minimum detectable surface concentration at the spacecraft (S/C) altitude. The different species happen to have similar densities at 100 km.

Table 2
Globally-averaged densities at 100 km altitude.

H ₂ O ^a	10^4 – 2×10^5 cm ⁻³
O ₂ ^a	4×10^6 – 10^7 cm ⁻³
H ₂ ^a	10^6 cm ⁻³
O ^a	3×10^4 – 10^5 cm ⁻³
OH ^a	10^2 – 9×10^4 cm ⁻³
Na ^b	60–1600 cm ⁻³
CO ₂ ^c	36–193 cm ⁻³
SO ₂ ^c	110–600 cm ⁻³

^a The ranges come from the differing results of Shematovich et al. (2005) and Smyth and Marconi (2006).

^b The range in Na density come from the observationally-constrained range in Na source rates estimated by Leblanc et al. (2005).

^c The ranges for SO₂ and CO₂ are based on the various scenarios discussed in the text.

composition and atmospheric dynamics. In spite of these uncertainties, it appears there are compelling reasons to have a mass spectrometer on a Europa orbiter.

Acknowledgments

T.A.C. wishes to acknowledge helpful discussions with Hunter Waite and Peter Wurz. T.A.C.'s work was supported with a NASA Graduate Student Research Program fellowship through the Langley Research Center and a fellowship from the Virginia Space Grant Consortium. R.E.J. acknowledges support from NASA's Planetary Atmospheres and Planetary Geology and Geophysics Programs.

References

- Bringa, E.M., Johnson, R.E., Jakas, M., 1999. Molecular-dynamics simulations of electronic sputtering. *Phys. Rev. B* 60, 15107–15116.
- Brown, M.E., 2001. Potassium in Europa's atmosphere. *Icarus* 151, 190–195.
- Brown, M.E., Hill, R.E., 1996. Discovery of an extended sodium atmosphere around Europa. *Nature* 380, 229–231.
- Burger, M.H., Johnson, R.E., 2004. Europa's neutral cloud: Morphology and comparison to Io. *Icarus* 171, 557–560.
- Carlson, R.W., 2001. Spatial distribution of carbon dioxide, hydrogen peroxide, and sulfuric acid on Europa. *Bull. Am. Astron. Soc.* 33, 1125.
- Carlson, R.W., 2004. Distribution of hydrogen peroxide, carbon dioxide, and sulfuric acid in Europa's icy crust. In: Workshop on Europa's Icy Shell: Past, Present, and Future. 7031.
- Carlson, R.W., Johnson, R.E., Anderson, M.S., 1999. Sulfuric acid on Europa and the radiolytic sulfur cycle. *Science* 286, 97–99.
- Carlson, R.W., Anderson, M.S., Mehlman, R., Johnson, R.E., 2005. Distribution of hydrate on Europa: Further evidence for sulfuric acid hydrate. *Icarus* 177, 461–471.
- Carlson, R.W., Calvin, W., Dalton, J.B., Hansen, G.B., Hudson, R., Johnson, R.E., McCord, T.B., Moore, M.H., 2009. Europa's surface composition: What we know, what we would like to know, and how we can find out. In: Pappalardo, R.T., McKinnon, W.B., Khurana, K.K. (Eds.), *Europa*. In press.
- Cassidy, T.A., Johnson, R.E., 2005. Monte Carlo model of sputtering and other ejection processes within a regolith. *Icarus* 176, 499–507.
- Cassidy, T.A., Johnson, R.E., McGrath, M.A., Wong, M.C., Cooper, J.F., 2007. The spatial morphology of Europa's near-surface O₂ atmosphere. *Icarus* 191, 755–764.
- Cassidy, T.A., Johnson, R.E., Geissler, P.E., Leblanc, F., 2008. Simulation of Na D emission near Europa during eclipse. *J. Geophys. Res. (Planets)* 113, doi:10.1029/2007JE002955. E02005.
- Cipriani, F., Leblanc, F., Witasse, O., Johnson, R.E., 2008. Sodium recycling at Europa: What do we learn from the sodium cloud variability? *Geophys. Res. Lett.* 35, doi:10.1029/2008GL035061. L19201.
- Cooper, J.F., Johnson, R.E., Mauk, B.H., Garrett, H.B., Gehrels, H., 2001. Energetic ion and electron irradiation of the icy Galilean satellites. *Icarus* 149, 133–159.
- Cosby, P.C., 1993. Electron-impact dissociation of oxygen. *J. Chem. Phys.* 98, 9560.
- Hall, D.T., Strobel, D.F., Feldman, P.D., McGrath, M.A., Weaver, H.A., 1995. Detection of an oxygen atmosphere on Jupiter's moon Europa. *Nature* 373, 677.
- Hall, D.T., Feldman, P.D., McGrath, M.A., Strobel, D.F., 1998. The far-ultraviolet oxygen airglow of Europa and Ganymede. *Astrophys. J.* 499, 475–481.
- Hand, K.P., Chyba, C.F., Carlson, R.W., Cooper, J.F., 2006. Clathrate hydrates of oxidants in the ice shell of Europa. *Astrobiology* 6 (3), 463–482.
- Hansen, G.B., McCord, T.B., 2008. Widespread CO₂ and other non-ice compounds on the anti-jovian and trailing sides of Europa from Galileo/NIMS observations. *Geophys. Res. Lett.* 35, doi:10.1029/2007GL031748. 1202.
- Hibbitts, C.A., Szanyi, J., McCord, T.B., 2004. Carbon dioxide in the surfaces of the icy satellites. *Bull. Am. Astron. Soc.* 36, 1123.
- Hodges Jr., R.R., 1980. Lunar cold traps and their influence on argon-40. *Lunar Planet. Sci. 11*, 2463–2477.
- Hudson, J.E., Vallance, C., Harland, P.W., 2004. Absolute electron-impact ionization cross sections for CO, CO₂, OCS and CS₂. *J. Phys. B* 37, 445.
- Itikawa, Y., Mason, N., 2005. Cross sections for electron collisions with water molecules. *J. Phys. Chem. Ref. Data* 34, 1–22.
- Jakas, M.M., Bringa, E.M., Johnson, R.E., 2002. Fluid dynamics calculation of sputtering from a cylindrical thermal spike. *Phys. Rev. B* 65, 165425.
- Johnson, R.E., 1990. Energetic Charged-Particle Interactions with Atmospheres and Surfaces. Springer-Verlag, Berlin.
- Johnson, R.E., 2000. Note: Na at Europa. *Icarus* 143, 429–433.
- Johnson, R.E., Killen, R.M., Waite, J.H., Lewis, W.S., 1998. Europa's sputter produced ionosphere. *Geophys. Res. Lett.* 25, 3257–3260.
- Johnson, R.E., Leblanc, F., Yakshinskiy, B.V., Madey, T.E., 2002. Energy distributions for desorption of sodium and potassium from ice: The Na/K ratio at Europa. *Icarus* 156, 136–142.
- Johnson, R.E., Quickenden, T.L., Cooper, P.D., McKinley, A.J., Freeman, C., 2003. The production of oxidants in Europa's surface. *Astrobiology* 3, 823–850.
- Johnson, R.E., Carlson, R.W., Cooper, J.F., Paranicas, C., Moore, M.H., Wong, M.C., 2004. Radiation effects on the surface of the Galilean satellites. In: Bagenal, F., Dowling, T., McKinnon, W.B. (Eds.), *Jupiter—The Planet, Satellites and Magnetosphere*. Cambridge Univ. Press, Cambridge. Chapter 20, pp. 485–512.
- Johnson, R.E., Burger, M.H., Cassidy, T.A., Smyth, W.H., Marconi, M.L., 2009. Modeling Europa's tenuous atmosphere. In: Pappalardo, R.T., McKinnon, W.B., Khurana, K.K. (Eds.), *Europa*. In press.
- Johnston, A.R., Burrow, P.D., 1995. Electron-impact ionization of Na. *Phys. Rev. A* 51, R1735–R1737.
- Kliore, A.J., Hinson, D.P., Flasar, F.M., Nagy, A.F., Cravens, T.E., 1997. The ionosphere of Europa from Galileo radio occultations. *Science* 277, 355–358.
- Lane, A.L., Nelson, R.M., Matson, D.L., 1981. Evidence for sulfur implantation in Europa's UV absorption band. *Nature* 292, 38.
- Leblanc, F., Johnson, R.E., Brown, M.E., 2002. Europa's sodium atmosphere: An ocean source? *Icarus* 159, 132–144.
- Leblanc, F., Potter, A.E., Killen, R.M., Johnson, R.E., 2005. Origins of Europa Na cloud and torus. *Icarus* 178, 367–385.
- Liang, M.C., Lane, B.F., Pappalardo, R.T., Allen, M., Yung, Y.L., 2005. Atmosphere of Callisto. *J. Geophys. Res. (Planets)* 110, 2003.
- Lindsay, B.G., Straub, H.C., Smith, K.A., Stebbings, R.F., 1996. Absolute partial cross sections for electron impact ionization of SO₂ from threshold to 1000 eV. *J. Geophys. Res.* 101, 21151–21156.
- Mauk, B.H., Mitchell, D.G., Krimigis, S.M., Roelof, E.C., Paranicas, C.P., 2003. Energetic neutral atoms from a trans-Europa gas torus at Jupiter. *Nature* 421, 920–922.
- McEwen, A.S., 1986. Exogenic and endogenic albedo and color patterns on Europa. *J. Geophys. Res.* 91, 8077–8097.
- Ockert, M.E., Nelson, R.M., Lane, A.L., Matson, D.L., 1987. Europa's ultraviolet absorption band (260 to 320 nm)—Temporal and spatial evidence from IUE. *Icarus* 70, 499–505.
- Orlando, T.M., McCord, T.B., Grieves, G.A., 2005. The chemical nature of Europa surface material and the relation to a subsurface ocean. *Icarus* 177, 528–533.
- Pappalardo, R.T., and 18 colleagues, 2007. Europa Explorer: A mission to explore Europa and investigate its habitability. *Bull. Am. Astron. Soc.* 39, Abstract #28.02.
- Paranicas, C., Ratliff, J.M., Mauk, B.H., Cohen, C., Johnson, R.E., 2002. The ion environment near Europa and its role in surface energetics. *Geophys. Res. Lett.* 29, 050000-1.
- Pospieszalska, M.K., Johnson, R.E., 1989. Magnetospheric ion bombardment profiles of satellites: Europa and Dione. *Icarus* 78, 1–13.
- Reimann, C.T., Boring, J.W., Johnson, R.E., Garrett, J.W., Farmer, K.R., Brown, W.L., 1984. Ion-induced molecular ejection from D₂O ice. *Surf. Sci.* 147, 227–240.
- Sandford, S.A., Allamandola, L.J., 1993. The condensation and vaporization behavior of ices containing SO₂, H₂S, and CO₂—Implications for Io. *Icarus* 106, 478–488.
- Saur, J., Strobel, D.F., Neubauer, F.M., 1998. Interaction of the jovian magnetosphere with Europa: Constraints on the neutral atmosphere. *J. Geophys. Res.* 103, 19947–19962.
- Shematovich, V.I., Johnson, R.E., Cooper, J.F., Wong, M.C., 2005. Surface bound atmosphere of Europa. *Icarus* 173, 480–498.
- Shi, J., Teolis, B.D., Baragiola, R.A., 2007. Irradiation enhanced adsorption and trapping of O₂ on microporous water ice. *Bull. Am. Astron. Soc.* 39, Abstract #38.04.
- Sieveka, E.M., Johnson, R.E., 1982. Thermal- and plasma-induced molecular redistribution on the icy satellites. *Icarus* 51, 528–548.
- Simonelli, D.P., Buratti, B.J., 2004. Europa's opposition surge in the near-infrared: Interpreting disk-integrated observations by Cassini VIMS. *Icarus* 172, 149–162.
- Sittler, E.C., Andre, N., Blanc, M., Burger, M., Johnson, R.E., Coates, A., Rymer, A., Reisenfeld, D., Thomsen, M.F., Persoon, A., Dougherty, M., Smith, H.T., Baragiola, R.A., Hartle, R.E., Chornay, D., Shappirio, M.D., Simpson, D., McComas, D.J., Young, D.T., 2008. Ion and neutral sources and sinks within Saturn's inner magnetosphere: Cassini results. *Planet. Space Sci.* 56, 3–18.
- Smyth, W.H., Marconi, M.L., 2006. Europa's atmosphere, gas tori, and magnetospheric implications. *Icarus* 181 (2), 510–526.
- Spencer, J.R., Tamppari, L.K., Martin, T.Z., Travis, L.D., 1999. Temperatures on Europa from Galileo PPR: Nighttime thermal anomalies. *Science* 284, 1514–1516.
- Steklov, A.F., 1977. Atmospheres of planetary satellites. I. Possibility of existence. *Astron. Vestnik* 1977, 219–225.
- Straub, H.C., Renault, P., Lindsay, B.G., Smith, K.A., Stebbings, R.F., 1996. Absolute partial cross sections for electron-impact ionization of H₂, N₂, and O₂ from threshold to 1000 eV. *Phys. Rev. A* 54, 2146–2153.
- Tiscareno, M.S., Geissler, P.E., 2003. Can redistribution of material by sputtering explain the hemispheric dichotomy of Europa? *Icarus* 161, 90–101.
- Tucker, O.J., Ivanov, D.S., Zhigilei, L.V., Johnson, R.E., Bringa, E.M., 2005. Molecular dynamics simulation of sputtering from a cylindrical track: EAM versus pair potentials. *Nucl. Instrum. Methods Phys. Res. B* 228, 163–169.
- Volwerk, M., Kivelson, M.G., Khurana, K.K., 2001. Wave activity in Europa's wake: Implications for ion pickup. *J. Geophys. Res.* 106, 26033–26048.
- Yung, Y.L., McElroy, M.B., 1977. Stability of an oxygen atmosphere on Ganymede. *Icarus* 30, 97–103.